Research Report - RH-4-23 *Icelandic Student Innovation Fund*

Using SAR images and pixel tracking to study large-scale motion of the Tungnakvíslarjökull landslide in Iceland

Ylse Anna de Vries

Master student in geophysics - University of Iceland

Supervised by:

Halldór Geirsson - University of Iceland

Co-supervised by:

Þorsteinn Sæmundsson - University of Iceland

Vincent Drouin - Icelandic Meteorological Office

September 26, 2023

HÁSKÓLI ÍSLANDS

Abstract

Large-scale landslides in Iceland are a major hazard threatening public safety. They require continuous monitoring to provide early warning and study their evolution. In this project a new method of observation using SAR satellite based pixel tracking is implemented and tested on the landslide area near Tungnakvíslarjökull, on the west flank of Katla volcano. A python-based data processing pipeline using the ISCE and AutoRIFT software is used to study TerraSAR-X data from 2010 to 2023, and results are published to a web application. The horizontal velocity of the landslide decreases from (5 ± 1) m yr^{-1} between 2010 to 2011 to (1 ± 1) m yr^{-1} from 2011 onward. A section of the landslide is observed moving to the east in 2011 to 2015, which not shown in other studies. This study shows that pixel tracking methods can provide significant and novel results for monitoring large-scale landslides in Iceland.

Acknowledgements

This project was funded by a the Icelandic Student Innovation Fund (Nýsköpunarsjóður námsmanna) of Rannís (Rannsóknamiðstöð Íslands), grant number: 2311501-1101. The project was also supported by the Institute of Earth Sciences, University of Iceland.

Special thanks to my supervisors, Halldór Geirsson, Þorsteinn Sæmundsson and Vincent Drouin. Thanks must also be extended to the Deformation Working Group at the Institute of Earth Sciences, and finally Reyn Alpha Magnúsar for lending their expertise in web development.

Table of contents

1 Introduction

Landslides throughout Iceland have had extensive effects on public safety and the natural environment, with road damages, fjord-amplified tsunamis and, when landslides interact with glaciers, jökulhlaups as potentially far-reaching consequences of these landslides (Sæmundsson et al. 2007; Lacroix et al. 2022; Dabiri et al. 2020). It is therefore of critical importance to monitor these landslides as completely as possible. Deformation techniques to monitor landslide motion include satellite based optical tracking, ground-based (continuous) GPS measurements and InSAR (see section 1.1.2) as examples of what is already being used to study these potential hazards.

The goal of this project is to attempt to extend this toolkit of monitoring methods by testing pixel tracking, where land deformation is measured by tracking individual pixels between an satellite image pair (Cai, Wang, et al. 2017), on a landslide area in Iceland. The project will particularly focus on applications of pixel tracking in satellite based Synthetic Aperture Radar (SAR) imagery, as this is generally weather-independent and widely available for land deformation monitoring in Iceland. Conventionally, SAR data has much been used for interferometric differencing (Simons and Rosen 2015), however, pixel tracking on SAR data has not been widely used in Iceland.

A pixel tracking data processing pipeline implementing python scripts, SAR processing and pixel tracking frameworks was created. This pipeline was tested on a landslide area around Tungnakvíslarjökull, on the western flank of Katla volcano. These results are subsequently made public using a newly built web application.

The following sections will briefly introduce the principles of SAR observations, the various SAR missions used in this project, the principles of pixel tracking and the landslide area studied in this project.

1.1 Synthetic Aperture Radar

Synthetic Aperture Radar (SAR) is an active imaging method using microwave radiation. The general principle involves the instrument emitting a pulse and then measuring using its antenna the radar reflections returned by the surface. These 'echos' do not return at the same time and by post-processing this time-dependent response an aperture (or viewing window) can be constructed. This process is repeated many time for a single SAR image.

SAR instruments are typically used for satellite-based Earth observation but ground and aircraft based implementations are also in use. This project will solely focus on space-based SAR observations. Microwave radiation experiences considerably less atmospheric interference (e.g. blocking by cloud cover) than optical wavelengths; it is therefore especially useful for long term ground deformation studies. The amplitude of the signal can be used for straight-forward imaging, but using the Interferometric SAR (InSAR, section 1.1.2) technique, even more information can be unlocked from the microwave echo (Pedersen and Freysteinn Sigmundsson 2006; Simons and Rosen 2015).

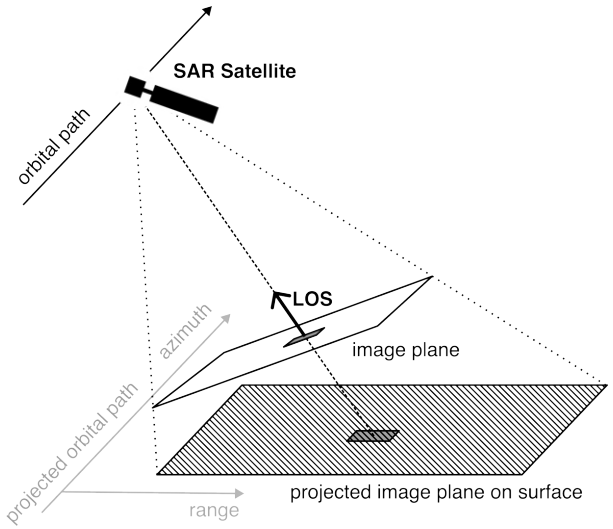

Figure 1.1: A diagram showing the geometry of SAR observations. Note how the image plane is tilted with respect to the ground plane and offset from the orbital path because of the side-looking viewing geometry of the satellite. The main axes relevant for SAR observations, range and azimuth are also shown. The Line of Sight (LOS) vector for a given pixel in the image is also shown (Simons and Rosen 2015).

The basic geometry of SAR observations is shown in Figure 1.1. SAR instruments have to observe at a look angle different to vertical with respect to their orbital path, typically from 15 to 40 degrees. Additionally, SAR satellites have polar orbits, orbits which cross the geographic poles during each rotation of the satellites, meaning their paths are generally oriented north-south. Combining these two elements, any SAR observation is never oriented exactly north-south, west-east or up-down, and these misalignments can not be straightforwardly accounted for.[1] Therefore any SAR observation is given in 'near' any given coordinate (e.g. near-north, near-east, near-up). This becomes especially relevant when discussing InSAR, which can only see deformation in the LOS direction, but when using pixel tracking we are seeing displacement in the image plane,

[1] For any given observation, insufficient parameters are known to solve for true geographic axes

perpendicular to the LOS.

1.1.1 — Satellite missions and instruments

Space-based SAR has been extensively used since the 1990s for ground deformation studies (Vadon and Sigmundsson 1997; Simons and Rosen 2015). Over the last three decades the imaging instruments have changed significantly. For this project we consider multiple satellite missions, see Table 1.1, with two distinct instruments: the AMI instrument (or derivatives) as used during the ERS1, ERS2 and Envisat missions (Attema 1991), used in various iterations from 1991 to 2012, and the SAR sensor on board the TerraSAR-X mission, in current use since 2007 (Fornaro, Reale, and Verde 2012; Symbios n.d.). The primary difference, relevant for pixel tracking, between these two instruments is the resolution, or ground coverage per pixel, of either instrument. While the resolution is roughly 30×30 m per pixel for the ERS sensors, it is roughly 1×1 m meter per pixel for the TerraSAR-X sensor (Table 1.1), due to very different mission designs and development of the technology over time.

Instrument	Mission	Start date	End date	Resolution (range x azimuth)	Reference
AMI	ERS-1	17-7-1991	07-3-2000	26 x 28 m	(Attema 1991)
	ERS-2	21-4-1995	04-7-2011	26 x 28 m	
ASAR	Envisat	01-3-2002	08-4-2012	26 x 28 m (AMI compatible)	(*ASAR Overview* n.d.)
C-Band SAR	Sentinel 1	03-4-2014	*present*	5 x 20 m	(Torres et al. 2012)
X-band SAR	TerraSAR-X	15-6-2007	*present*	0.59 x 1.1 m	(Fornaro, Reale, and Verde 2012)
SAR 2000	COSMO-SkyMed	08-6-2007	*present*	3 x 3 m	(*COSMO-SkyMed* n.d.)

Table 1.1: Overview of SAR satellite missions and instruments considered in this project. Grayed-out rows refer to missions not included in this project but that may be relevant for comparison. Dates are taking from the CEOS database (`https://ceos.org/`).

1.1.2 — Interferometric SAR

Interferometric SAR (InSAR) is an imaging technique that uses the constructive and destructive interference of the electromagnetic waves observed by the SAR instrument to detect changes in these patterns between two repeated image passes over time. This results in an interferogram image that can allow us to view ground deformation on the order of the wavelength of microwave radiation, i.e. centimetres in the LOS direction (Simons and Rosen 2015). This technique is not used in this project but it should be noted that InSAR can be supplemented with pixel tracking techniques as InSAR may be unable correlate large deformation where pixel tracking techniques will still be able to maintain coherence (Barnhart, Hayes, and Gold 2019).

1.1.3 — Pixel tracking

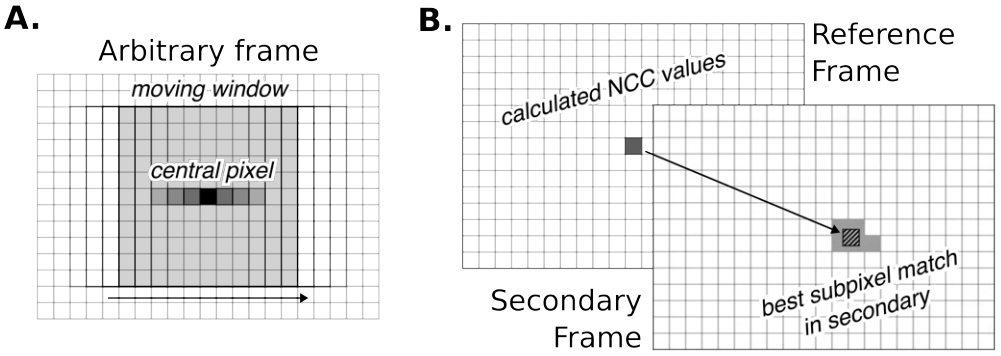

Figure 1.2: A diagram showing: (A.) How a correlation window (of $M \times N$ size) moves across an image to calculate the normalized cross correlation function for each pixel, and (B.) How these cross correlation function values can then be compared per images to generate a per pixel subpixel displacement between two (reference, primary) frames (Cai, Wang, et al. 2017).

Pixel tracking is an image processing technique that tracks per-pixel movement between image pairs, using automated methods. A similar manual technique is called feature tracking, where recognisable objects are tracking over image pairs. Notably, using specific algorithms sub-pixel accuracy can be obtained for any given image (Cai, Wang, et al. 2017). Pixel tracking is not just limited to SAR imagery, it can be used for all images showing displacements of clusters of pixels.

A well established pixel tracking algorithm is the Normalised Cross Correlation (NCC) algorithm. In it's most basic form it calculates correlation functions over two images for a moving $M \times N$ sized window centred on every pixel in the image (Figure 1.2). It then searches, within a reasonable search window, for the highest correlation between a reference pixel and an area within the secondary image. The principle of this technique is shown in Figure 1.2, although it should be noted that the matching methods within the NCC algorithm can increase in complexity, to enable sub-pixel accuracy. Image resolution is a notably large limitation for accurate pixel tracking results, in addition to noise and image distortion (Debella-Gilo and Kääb 2011). Many SAR processing frameworks incorporate pixel tracking programs to enable InSAR processing (*ISCE* n.d.; *AutoRIFT* n.d.). For large images the correlation function calculations have to be repeated significantly often, therefore pixel tracking implementations benefit a lot from computational optimisation.

For specifically landslide monitoring using SAR images, alternatives for the NCC algorithm have been developed (Cai, Zhang, et al. 2022) and should be noted to increase accuracy. They are not used in this project, as they are generally not easily available and computationally optimised, prohibiting experimentation, as is the goal for this exploratory study.

1.2 Landslide study area - Tungnakvíslarjökull

In this project the landslide north of Tungnakvíslarjökull is used as a primary study area. As described in Lacroix et al. (2022), Saemundsson, Páll Einarsson, et al. (2020), and Saemundsson, Pall Einarsson, et al. (2021), the landslide area is located on the slope to the north of Tungnakvíslarjökull glacier, which is an outlet glacier of Mýrdalsjökull, see Figure 1.3 for an overview of the area.

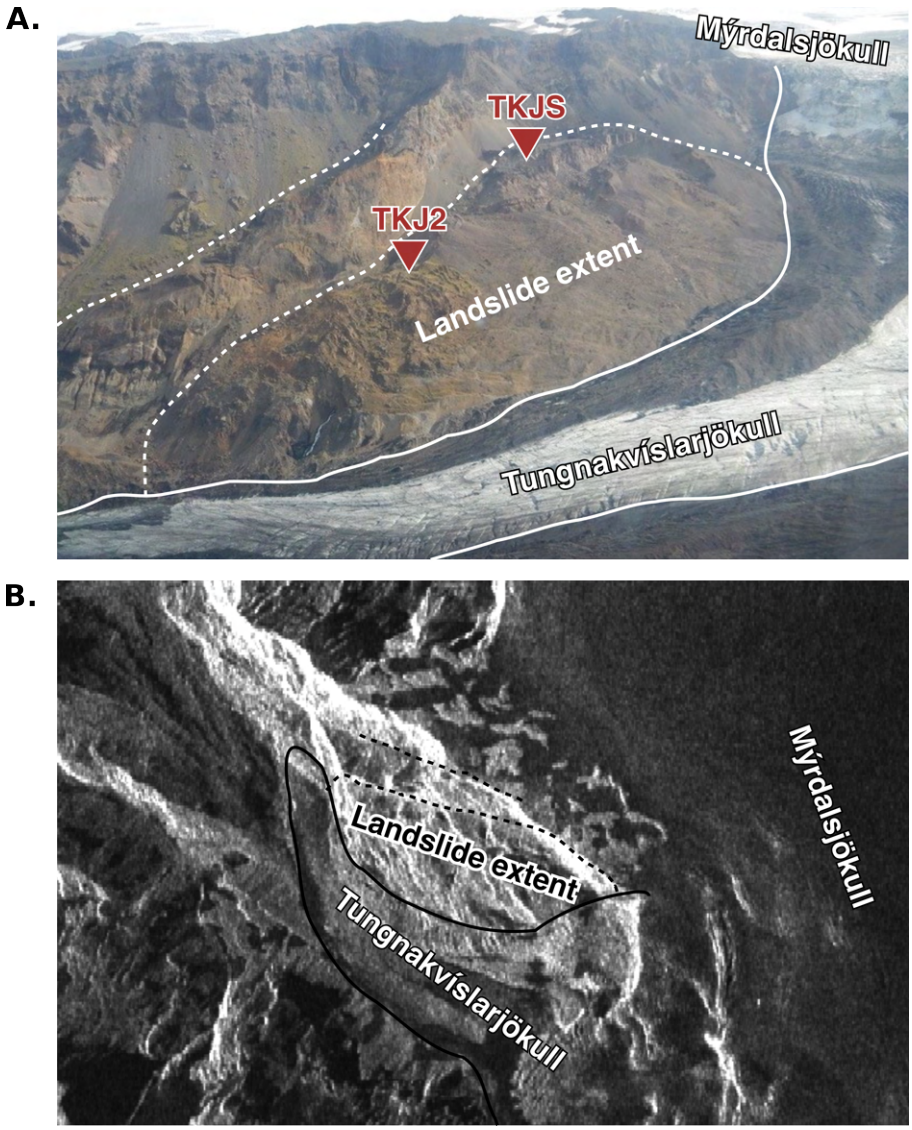

Figure 1.3: An overview of the study area of this project, the landslide near Tungnakvíslarjökull: (A.) is a photograph by Halldór Geirsson taken in August 2019 showing the landslide area, including some notations. Also included are the locations of the two contintuous GPS stations TKJS and TKJ2 (Geirsson et al. 2023). (B.) is a SAR image from the TerraSAR-X satellite observed on 20-06-2020 with similar annotations.

This northern slope of the valley consists of rhyolitic lavas capped by hyaloclastite and is notably unstable. The landslide has been active since at least 1945 with a notable acceleration between 2000 and 2004 (Lacroix et al. 2022) The landslide movement is most likely caused by the steady retreat of Tungkvíslarjökull due to climate change, consistent with glaciers all over Iceland (Saemundsson, Pall Einarsson, et al. 2021; Saemundsson, Páll Einarsson, et al. 2020). In august 2019 a continuous GPS station (TKJS) was installed on the landslide slopes, later supplemented by station (TKJ2) in June 2020 (see: `https://strokkur.raunvis.hi.is/gipsy/icel_tkjs.html`, Geirsson et al. (2023)), they show a general south- and westward down-slope movement of the landslide body. For the pixel tracking we expect to see similar trends within the movement of the entire landslide area.

2 Pixel tracking processing

2.1 Data

All data processed in this project was archived by the Earth Science Institute on their main InSAR processing server called *Dyngja*. TerraSAR-X data covering Tungnakvíslarjökull was originally acquired for deformation studies in the Mýrdalsjökull area, focusing on the Katla volcano. All ERS-1 and ERS-2 data were complete survey tracks covering the whole of Iceland, which were stored for long-term access and historical data processing.

2.2 Overview

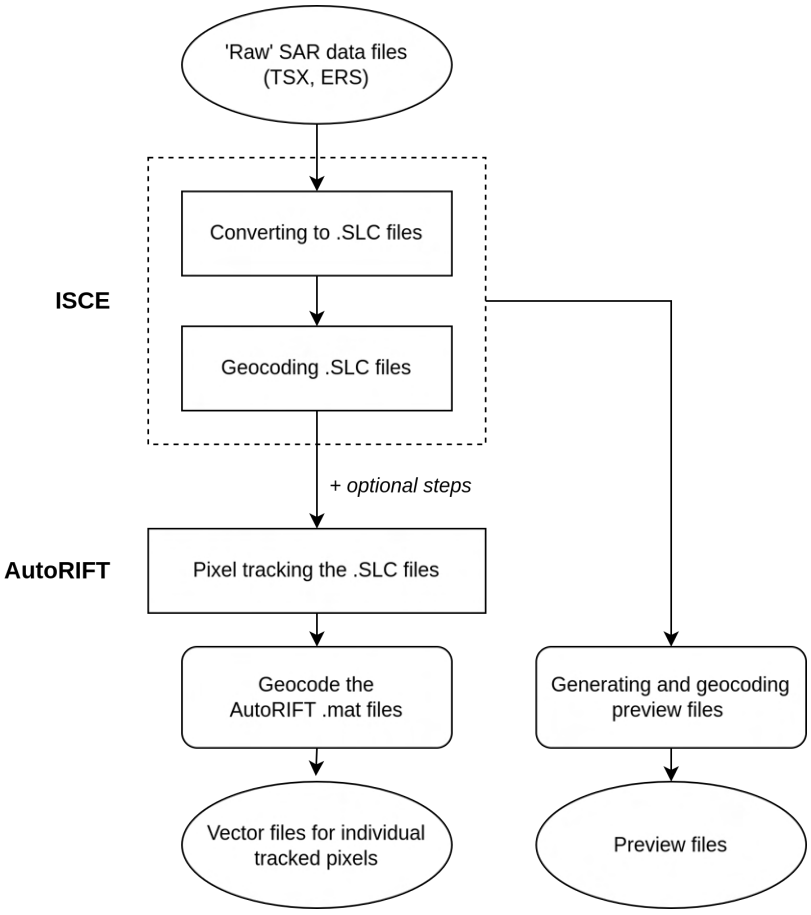

Figure 2.1: A schematic overview of the pixel tracking pipeline as implemented in this project.

The processing is done within a number of scripts in Python, version 3.11, that are run on the Dyngja computer. The scripts are run as a step-based 'pipeline' that generate intermediate files before eventually storing a number of data products (see details below). The main interface of the pipeline is built in analogue to the main processing of the ISCE framework. All scripts are made

publicly available on Github (`https://github.com/ylseanna/RANNIS2023PixelTracking`). A schematic overview of the processing can be found in Figure 2.1.

The main overarching python script prepares metadata for the SAR images and then runs progressively two external data frameworks: ISCE (v2.6.3) and AutoRIFT. ISCE (Interferometric synthetic aperture radar Scientific Computing Environment) is a widely used and well-established NASA-developed framework to process InSAR data (*ISCE* n.d.). ISCE's primary advantage for this project is that it is able to ingest many different satellite platform types in a unified approach. AutoRIFT (Autonomous Repeat Image Feature Tracking) in turn is a much newer project to implement fast and efficient pixel displacement between two images (*AutoRIFT* n.d.). AutoRIFT is built into newer versions of ISCE.

The pipeline is always run for two SAR images, a reference image and a secondary image, where the second is compared to the first. ISCE is initially run to translate and geocode the two SAR images provided to the pipeline. For SAR imagery ISCE uses a format called the Single Look Complex (SLC) which holds the both the amplitude and phase of the SAR data provided. Any 'raw' data provided to ISCE gets converted to SLC. ISCE then performs geocoding (also called geolocating) where every pixel in the SAR image, based on the orbital parameters of particular image and a provided Digital Elevation Model (DEM), is connected to a particular longitude, latitude and elevation. In this project the ÍslandsDEM by the National Land Survey of Iceland is used (`https://www.lmi.is/is/landupplysingar/gagnagrunnar/is-50v`). However, the geocoded data are not used for cross-correlation (see following paragraph). Also included in this data is the look angle with respect to the satellite for each pixel, and each pixel's heading.

AutoRIFT is then run to calculate the pixel displacement between the two images, it is able to use SLC images. This outputs a matrix file including the displacement in the x-axis and y-axis of the particular image. All these calculations are performed in the image frame, so no geographic data is yet included, and all displacements are given in pixels.

The pipeline then takes the output of AutoRIFT and applies the reference image geocoding from ISCE to each pixel displacement. Additionally, by calculating the total extent of the image and deriving from this a pixel to meter conversion, the pixel displacements are converted to metric displacements, in a near-horizontal frame tilted along the line-of-sight of the satellite. For each valid pixel in the displacement file the individual displacements are then stored in a comma-seperated-values (CSV) file, including pixel displacements (Dx, Dy), longitude, latitude, elevation (as derived from the DEM), and pixel heading and tilt with respect to the LOS.

Finally, all reference and secondary images are geolocated and projected using the GDAL software (Warmerdam and Rouault 1998) which provides 'preview' background images for verification of the vector data. All images are then copied and stored. The pipeline can then be repeated for any other two images.

3 Results

3.1 Performance of pixel tracking pipeline

When testing the pipeline on ERS-1 and ERS-2 data unfortunately no useful results were found for the landslide area. This is presumably due to insufficient resolution and too high noise for these images. TerraSAR-X data did give reasonable results. This implies that the 30 m resolution of the AMI instrument (ERS-1, ERS-2, Envisat's ASAR) is not sufficient for pixel tracking applications on landslide data, while TerraSAR-X 1 m resolution is sufficient (Table 1.1).

For the TerraSAR-X data an individual pipeline run for each time span would take roughly six minutes. Of these six minutes about four would be used by the ISCE pre-processing and geocoding steps, while AutoRIFT ran in roughly 20 seconds.

3.2 Results for Tungnakvíslarjökull

The pipeline was run for 7 TerraSAR-X frame pairs covering the Tungnakvíslarjökull area, spanning 21-6-2010 to 3-6-2023. Only the period between 25-6-2018 and 20-062020 failed to give results. Frames were selected to give roughly one year intervals.

Reference and secondary frames were generally not perfectly aligned and therefore had large, approximately 15 m, systemic displacements over the entire image. These were accounted for by subtracting the median of all pixel motions across the study area. Errors were estimated based on the 'background' movements seen in assumed non-moving areas surrounding the landslide, and are around 1 m, or notably roughly the pixel resolution, for each image pair.

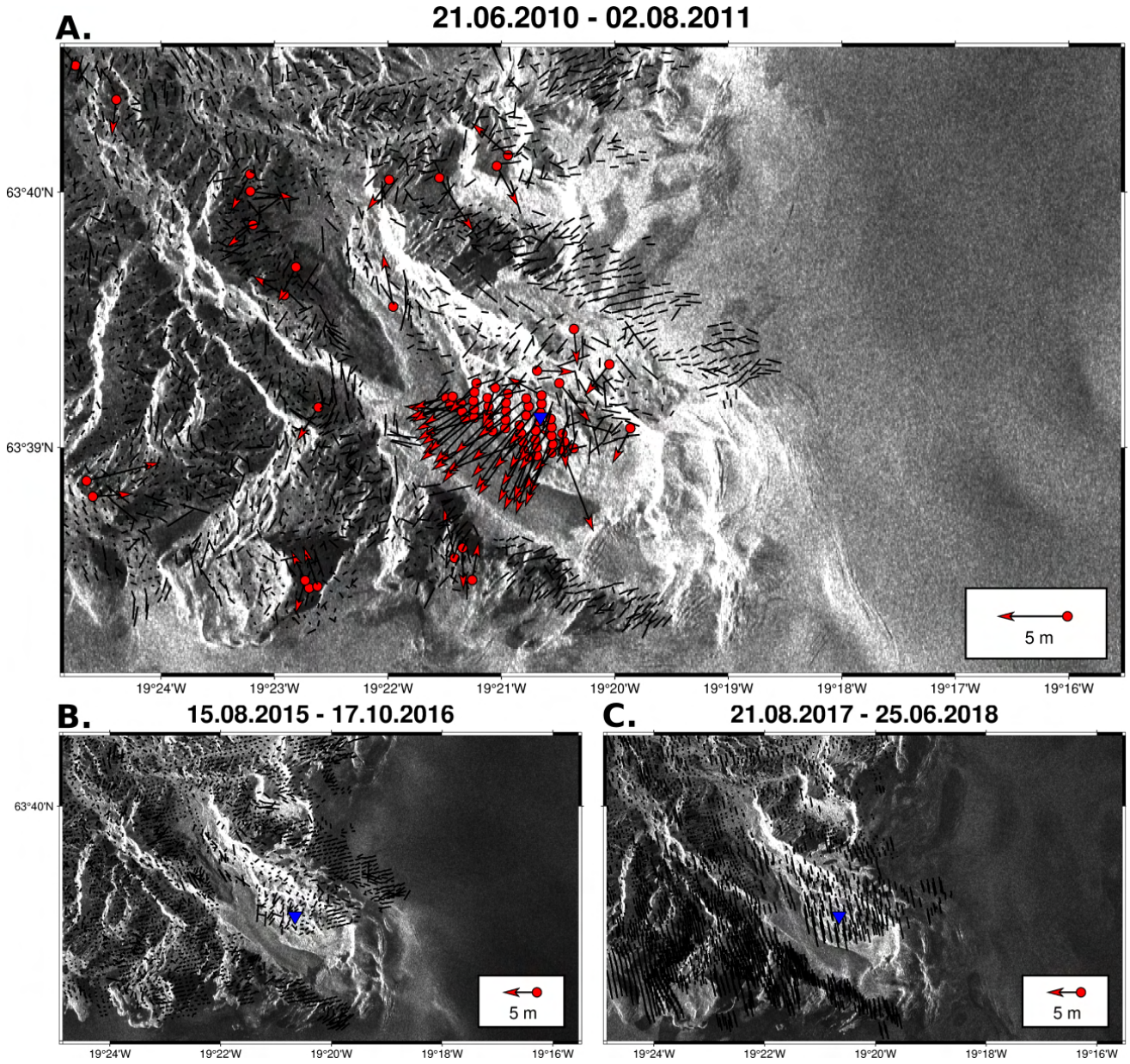

Figure 3.1: Per pixel near horizontal displacement plotted as vectors for the Tungnakvíslarjökull area. (A.) covers 21-06-2010 to 02-08-2011. Of all the periods studied this plot shows the largest displacement, and is a good illustration of the general trend with movement in the landslide area. (B.) shows a later timeframe where the movement has clearly decreased. (C.) shows how systematic errors can interfere with the processing. The blue triangle in each image shows the coordinates where the results were spatially interpolated, i.e. surrounding pixel points were combined and averaged to account for displacements vectors not always being co-located between images, to create a times series of horizontal velocity, see Figure 3.3.

A sample of the pixel tracking results is given in Figure 3.1, where one can see that especially for earlier periods with higher displacements the displacement vectors show a clear down-slope movement consistent with what we expect from the literature. Later periods show notably less movement within the landslide. The time period 21-08-2017 to 25-6-2018 (Figure 3.1 C.), seems to show a systemic error, most likely reflecting a poor representation of average movement by

the median value of motion. All displacement plots can be found full-sized in Appendix A.

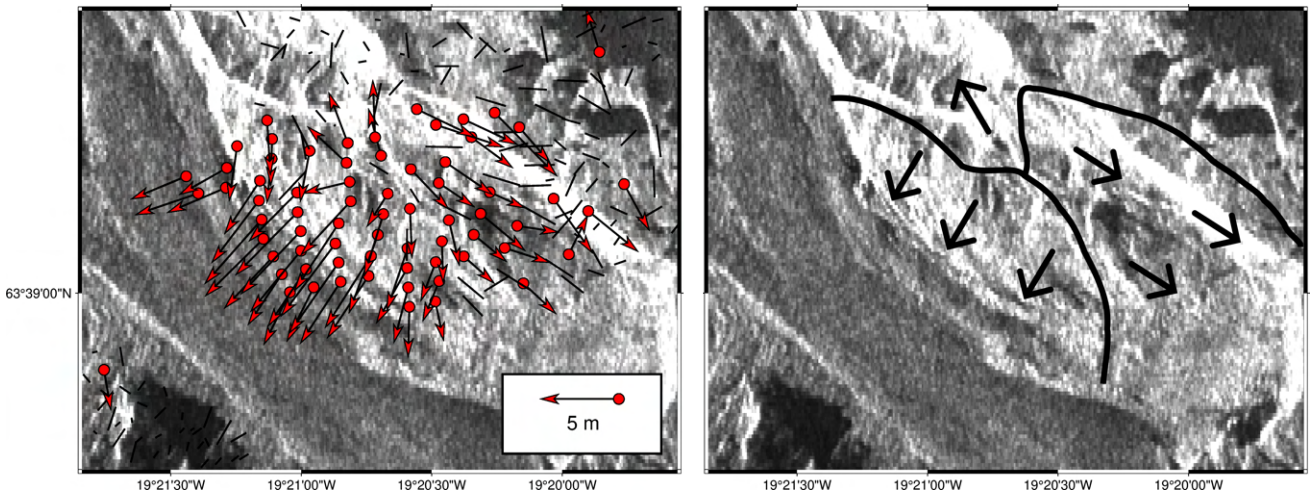

Figure 3.2: Per pixel near-horizontal displacement plotted as vectors for the Tungnakvíslarjökull area between 2-8-2011 and 15-8-2015. It shows an southeastward motion in the northeast portion of the landslide area.

The pixel displacement between 2-8-2011 and 15-8-2015 showed some interesting eastward motion in the northeastern part of the landslide area, illustrated in Figure 3.2. This shows that pixel tracking can reveal different blocks moving separately within a larger landslide.

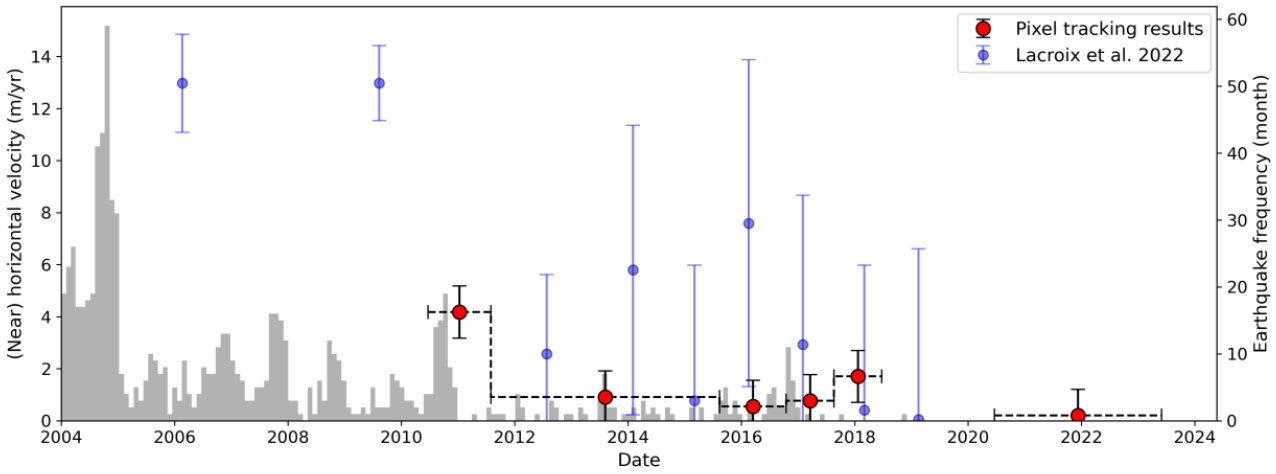

Figure 3.3: Interpolated near-horizontal velocity (or movement rate) for each time frame at the location marked with the blue triangle in Figure 3.1. In blue are shown horizontal velocity results from Lacroix et al. (2022). Gray histogram shows the monthly number of earthquakes from Lacroix et al. (2022).

Figure 3.3 shows the overall trend of near-horizontal velocity in the landslide for the pixel tracking results in this report. To calculate this surrounding pixel-wise displacements were combined and averaged (i.e. spatially interpolated) to account for pixel displacement vectors not always being co-located between images. Then the displacement was divided by the time span in years to calculate an average velocity. Finally, the x and y-components were combined to generate a

total velocity. The results are also compared to values published in Lacroix et al. (2022), which show a generally similar trend, but with slightly higher uncertainties. We can clearly see that the decrease in velocity after 2010 corresponds to a decrease in seismic activity in the area. As shown in Figure 3.1 C. the increase around 2018 is probably the result of a systematic error in the pixel tracking results.

4 Web Application

For public viewing of the pixel-tracking results, the output of the processing pipeline is hosted on a University of Iceland web server. The web application on the page is a client-side app written in next.js and uses a python-based flask Application Programming Interface (API) for server-side data accessing (source code: `https://github.com/ylseanna/PixelTrackingWebApp`).

The API allows the source data to be downloaded for use in other publications or web applications. Meanwhile, the web interface displays the pixel tracking results in a similar manner as the plots provided in this report. The website is hosted on the *strokkur* web server, at the address: `https://strokkur.raunvis.hi.is/pixeltracking/en/area/tungpt`.

The displayed and downloadable data is directly generated from output files of the pixel tracking pipeline and posted dynamically. The means that if the pipeline were to be run continually in the background with newly incoming SAR data, it would be possible to directly display the data on the web application.

5 Discussion

5.1 Pixel tracking pipeline

As noted in the section 3, the ISCE processing takes up a significant amount of time within the overall pipeline processing. AutoRIFT in turn runs incredibly quickly. This can be attributed to the fact that AutoRIFT is a much more modern and less rigid framework that has been optimised for pixel tracking specifically (Lei, Gardner, and Agram 2021). ISCE however, especially for this exploratory exercise, gives great flexibility when it comes to being able to switch between platforms to study. If the study of landslides using pixel tracking is continued, it might be beneficial to try to cut out the ISCE processing step, by switching to other processing frameworks.

The lack of results for ERS data may be attributed to simple resolution constraints within the AMI instrument (Table 1.1), but as AutoRIFT is a flexible method it may be possible to tweak its parameters, such as search window size, further to target ERS data better. Upon visual inspection ERS data did show a high noise level and significant variation between frames over time.

Generally the pipeline performed well for TerraSAR-X data, out-of-the-box, needing very little manual tweaking of parameters. This suggests that using pixel tracking for continued landslide monitoring, such as by automatically processing newly incoming frames has potential.

TerraSAR-X frames are, however, generally not acuired very regularly as the TerraSAR-X mission is not generally a monitoring mission. For this the on-going and publicly available Sentinel 1 mission is better suited, but its lower ground resolution (20 x 5 m, Table 1.1) may cause complications (Torres et al. 2012). It would however be a logical next mission to investigate, when it comes to continuous monitoring.

5.2 Tungnakvíslarjökull

The general agreement between the results from Lacroix et al. (2022) and the pixel tracking results in this project is notable (Figure 3.3), although it seems that (Lacroix et al. 2022) shows systemically higher expected ground movements after 2010. But the higher uncertainty for the Lacroix et al. (2022) data may account for this, while the pixel tracking results in this report have a significantly lower uncertainty. The pixel tracking results do constrain the slow down in 2010-2012 to more closely correspond with the decrease seismicity seen in the area (Figure 3.3), which would be expected if the ground movement was the cause of the seismic signal.

The eastward block wise movement seen in Figure 3.2 was not previously observed. The fact that it occurred only in a relatively brief period after the slow down in 2010-2012 may suggest some correlation between the two. Possibly the lower part of the landslide body obstructed further downward movement of the a higher part, causing it to briefly split and move down slope through a different path, until settling.

6 Conclusions

Pixel tracking in SAR images proves to be a viable method for landslide tracking. High resolution data is necessary, but will then also provide good spatial information for the evolution of the landslide. Older survey data (ERS-1, ERS-2, Envisat) does not seem of practical use. The processing pipeline is adaptable for multiple satellite missions, runs efficiently, and can be adapted for continuous monitoring through the web interface. Continued development of SAR Pixel Tracking methods should emphasise testing and applications for additional instruments, such as Sentinel 1 and COSMO-SkyMed, and may experiment with other algorithms.

The results for the landslide near Tungnakvíslarjökull confirm and refine the slowing down of landslide movement since 2004 and help constrain an additional deceleration period that coincides with reduced seismicity in 2011, as well as showing separate blocks moving within the landslide extent. SAR-based pixel tracking can therefore be added as a tool for large-scale landslide monitoring in Iceland.

Reykjavík, 26. september 2023

Bibliography

ASAR Overview (n.d.). https://earth.esa.int/eogateway/instruments/asar/description. Accessed: 2023-9-25. URL: https://earth.esa.int/eogateway/instruments/asar/description.

Attema, E P W (June 1991). “The Active Microwave Instrument on-board the ERS-1 satellite”. In: *Proc. IEEE* 79.6, pp. 791–799. ISSN: 1558-2256. DOI: 10.1109/5.90158. URL: http://dx.doi.org/10.1109/5.90158.

AutoRIFT (n.d.). en. https://github.com/nasa-jpl/autoRIFT. Accessed: 2023-5-18. URL: https://github.com/nasa-jpl/autoRIFT.

Barnhart, William D, Gavin P Hayes, and Ryan D Gold (Nov. 2019). “The July 2019 Ridgecrest, California, earthquake sequence: Kinematics of slip and stressing in cross-fault ruptures”. en. In: *Geophys. Res. Lett.* 46.21, pp. 11859–11867. ISSN: 0094-8276, 1944-8007. DOI: 10.1029/2019gl084741. URL: http://dx.doi.org/10.1029/2019gl084741.

Cai, Jiehua, Changcheng Wang, et al. (Aug. 2017). “An Adaptive Offset Tracking Method with SAR Images for Landslide Displacement Monitoring”. en. In: *Remote Sensing* 9.8, p. 830. ISSN: 2072-4292, 2072-4292. DOI: 10.3390/rs9080830. URL: https://www.mdpi.com/2072-4292/9/8/830.

Cai, Jiehua, Lu Zhang, et al. (Aug. 2022). “Polarimetric SAR pixel offset tracking for large-gradient landslide displacement mapping”. en. In: *Int. J. Appl. Earth Obs. Geoinf.* 112.102867, p. 102867. ISSN: 1569-8432, 1872-826X. DOI: 10.1016/j.jag.2022.102867. URL: http://dx.doi.org/10.1016/j.jag.2022.102867.

COSMO-SkyMed (n.d.). https://earth.esa.int/eogateway/missions/cosmo-skymed. Accessed: 2023-9-25. URL: https://earth.esa.int/eogateway/missions/cosmo-skymed.

Dabiri, Zahra et al. (Aug. 2020). “Assessment of Landslide-Induced Geomorphological Changes in Hıtardalur Valley, Iceland, Using Sentinel-1 and Sentinel-2 Data”. en. In: *NATO Adv. Sci. Inst. Ser. E Appl. Sci.* 10.17, p. 5848. ISSN: 0168-132X. DOI: 10.3390/app10175848. URL: https://www.mdpi.com/2076-3417/10/17/5848.

Debella-Gilo, Misganu and Andreas Kääb (Jan. 2011). “Sub-pixel precision image matching for measuring surface displacements on mass movements using normalized cross-correlation”. In: *Remote Sens. Environ.* 115.1, pp. 130–142. ISSN: 0034-4257. DOI: 10.1016/j.rse.2010.08.012. URL: https://www.sciencedirect.com/science/article/pii/S003442571000252X.

Fornaro, G, D Reale, and S Verde (Aug. 2012). “Potential of SAR for monitoring transportation infrastructures: An analysis with the multi-dimensional imaging technique”. In: *J. Geophys. Eng.* 9.4. ISSN: 1742-2132, 1742-2140. DOI: 10.1088/1742-2132/9/4/S1. URL: https://www.researchgate.net/publication/254502976_Potential_of_SAR_for_monitoring_transportation_infrastructures_An_analysis_with_the_multi-dimensional_imaging_technique.

Geirsson, Halldór et al. (Feb. 2023). *Seasonal and precipitation-triggered movements of the Almenningar and Tungnakvıslarjökull landslides, Iceland, monitored by low-cost GNSS observations*. Tech. rep. EGU23-13439. Copernicus Meetings. DOI: 10.5194/egusphere-egu23-13439. URL: https://meetingorganizer.copernicus.org/EGU23/EGU23-13439.html.

ISCE (n.d.). en. https://github.com/isce-framework/isce2. Accessed: 2023-5-18. URL: https://github.com/isce-framework/isce2.

Lacroix, Pascal et al. (July 2022). "Mechanisms of landslide destabilization induced by glacier-retreat on tungnakvıslarjökull area, Iceland". en. In: *Geophys. Res. Lett.* 49.14. ISSN: 0094-8276, 1944-8007. DOI: 10.1029/2022gl098302. URL: https://onlinelibrary.wiley.com/doi/10.1029/2022GL098302.

Lei, Yang, Alex Gardner, and Piyush Agram (Feb. 2021). "Autonomous Repeat Image Feature Tracking (autoRIFT) and Its Application for Tracking Ice Displacement". en. In: *Remote Sensing* 13.4, p. 749. ISSN: 2072-4292, 2072-4292. DOI: 10.3390/rs13040749. URL: https://www.mdpi.com/2072-4292/13/4/749.

Pedersen, Rikke and Freysteinn Sigmundsson (Feb. 2006). "Temporal development of the 1999 intrusive episode in the Eyjafjallajökull volcano, Iceland, derived from InSAR images". In: *Bull. Volcanol.* 68, pp. 377–393. ISSN: 0258-8900. DOI: 10.1007/s00445-005-0020-y. URL: https://ui.adsabs.harvard.edu/abs/2006BVol...68..377P.

Sæmundsson, Þ et al. (2007). "Monitoring of the Tjarnardalir landslide, in Central North Iceland". In.

Saemundsson, Thorsteinn, Pall Einarsson, et al. (Mar. 2021). *Deep seated gravitational slope deformation north of the Tungnakvıslarjökull outlet glacier, in western Mýrdalsjökull ice cap, S-Iceland*. Tech. rep. EGU21-14225. Copernicus Meetings. DOI: 10.5194/egusphere-egu21-14225. URL: https://meetingorganizer.copernicus.org/EGU21/EGU21-14225.html.

Saemundsson, Thorsteinn, Páll Einarsson, et al. (2020). "Slope deformation above the Tungnakvıslarjökull outlet glacier in western part of the Mýrdalsjökull glacier". In: Oslo, Norway.

Simons, M and P A Rosen (2015). "Interferometric Synthetic Aperture Radar Geodesy". In: *Treatise on Geophysics*. Elsevier, pp. 339–385. ISBN: 9780444538031. DOI: 10.1016/b978-0-444-53802-4.00061-0. URL: http://dx.doi.org/10.1016/B978-0-444-53802-4.00061-0.

Symbios (n.d.). *CEOS database*. URL: http://database.eohandbook.com/index.aspx.

Torres, Ramon et al. (May 2012). "GMES Sentinel-1 mission". In: *Remote Sens. Environ.* 120, pp. 9–24. ISSN: 0034-4257. DOI: 10.1016/j.rse.2011.05.028. URL: https://www.sciencedirect.com/science/article/pii/S0034425712000600.

Vadon, H and F Sigmundsson (Jan. 1997). "Crustal Deformation from 1992 to 1995 at the Mid-Atlantic Ridge, Southwest Iceland, Mapped by Satellite Radar Interferometry". en. In: *Science* 275.5297, pp. 193–197. ISSN: 0036-8075, 1095-9203. DOI: 10.1126/science.275.5297.194. URL: http://dx.doi.org/10.1126/science.275.5297.194.

Warmerdam, F and E Rouault (1998). *GDAL*. en. URL: https://gdal.org/.

Appendices

A TSX full size plots for Tungnakvíslarjökull

21.06.2010 - 02.08.2011

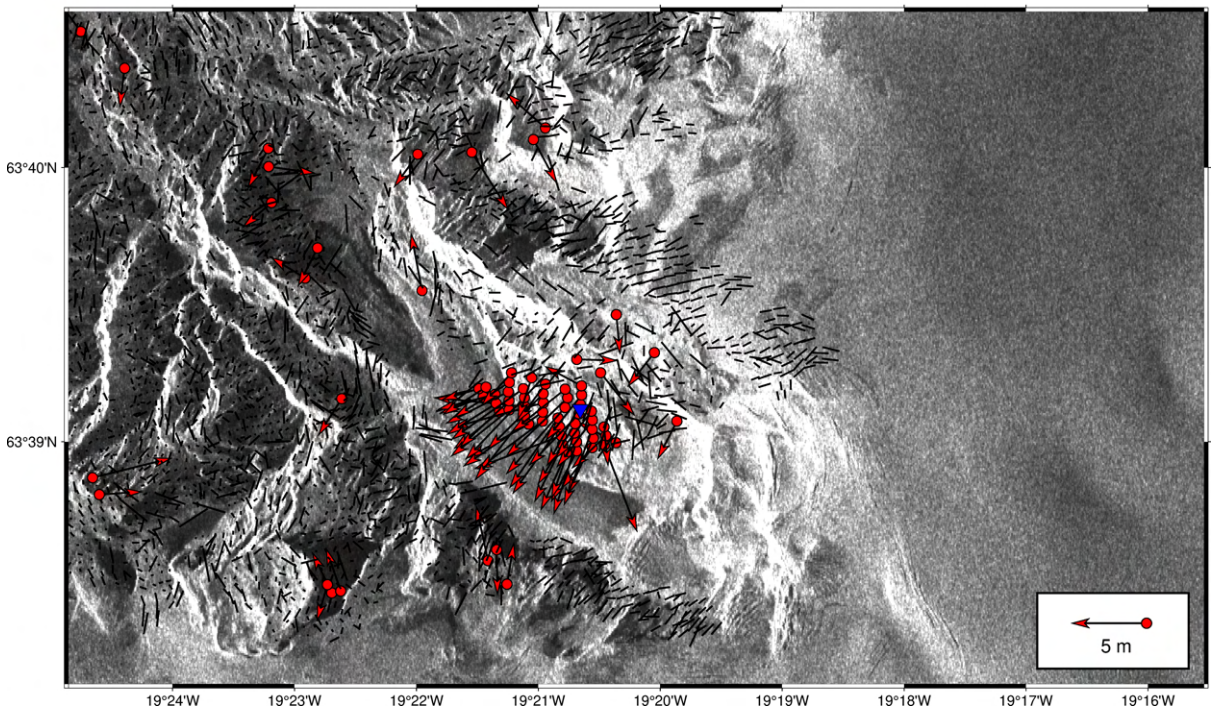

02.08.2011 - 15.08.2015

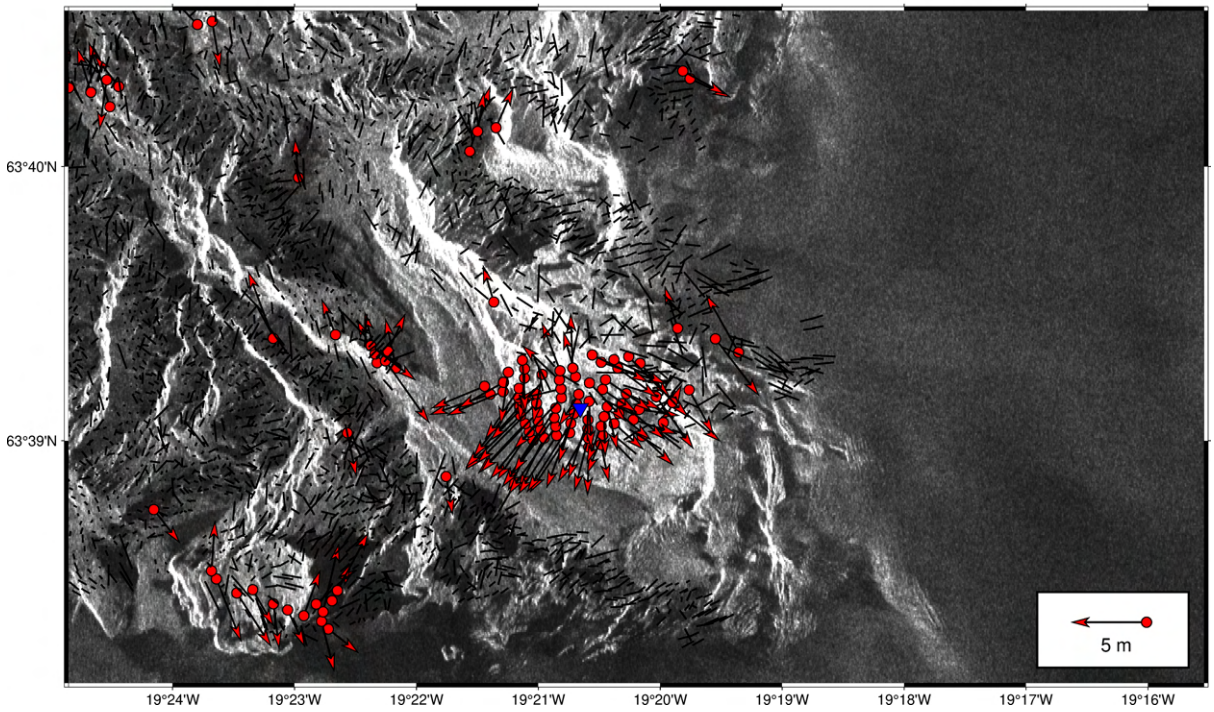

15.08.2015 - 17.10.2016

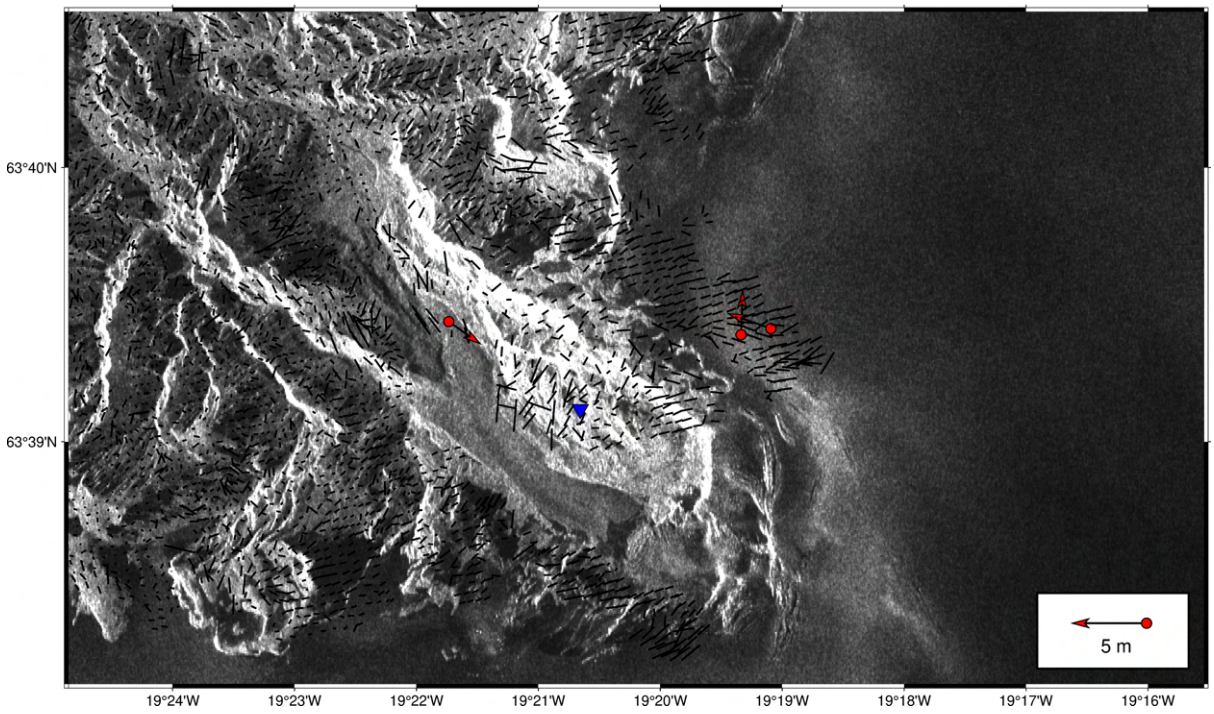

17.10.2016 - 21.08.2017

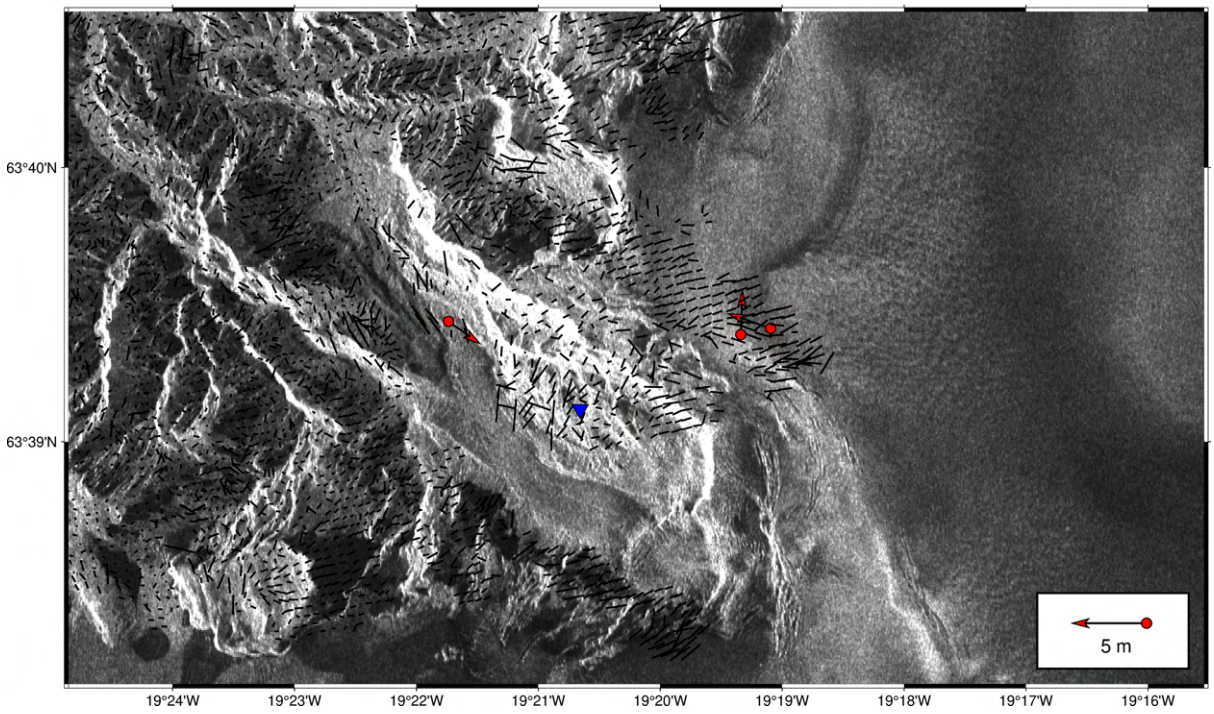

21.08.2017 - 25.06.2018

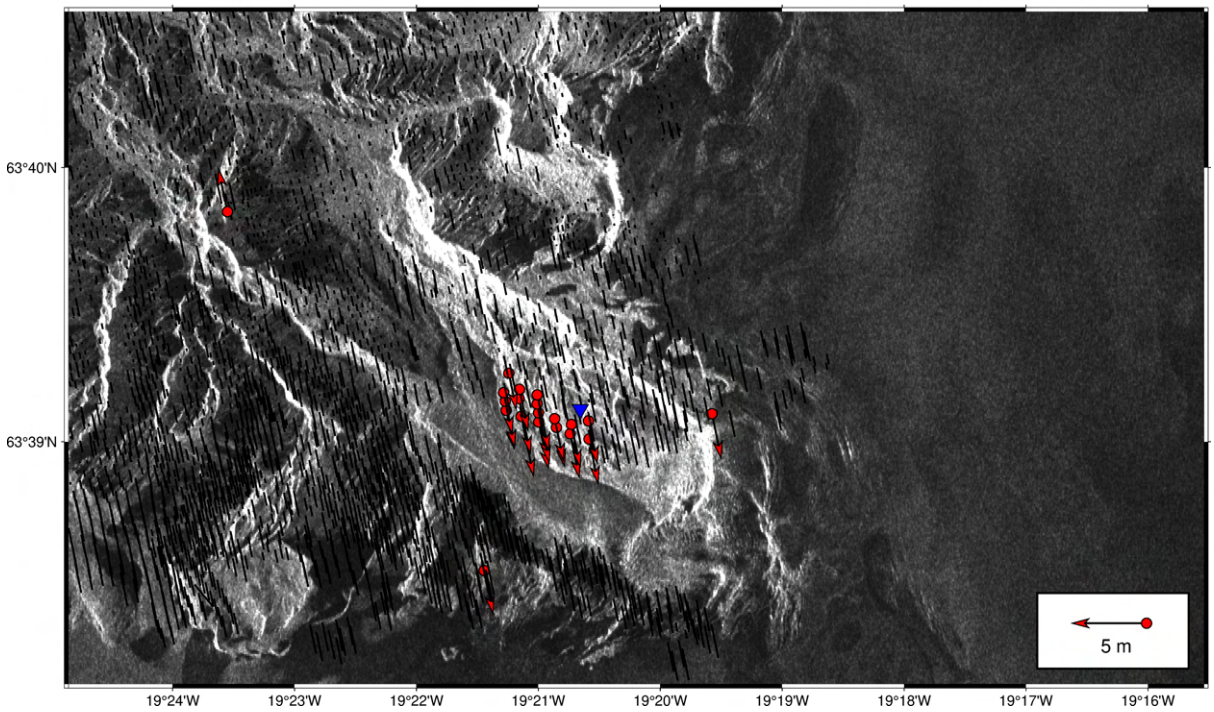

20.06.2020 - 03.06.2023